Physicochemical Investigations of the Basicity of the Cation Exchanged ETS-10 Molecular Sieves

Suresh B. Waghmode, Rajappan Vetrivel,† Suryakant G. Hegde, Chinnakonda S. Gopinath,* and Subramanian Sivasanker*

Catalysis Division, National Chemical Laboratory, Pune 411 008, India

Received: December 31, 2002; In Final Form: May 27, 2003

Alkali-metal exchanged M-ETS-10 (M= Li, Na, K, Rb, Cs, and Ba) molecular sieves have been investigated by different techniques such as X-ray diffraction, FTIR, TPD, and XPS. It is found that the overall Lewis basicity in M-ETS-10 increases as the cation is changed from Li to Cs in the alkali cation series. FTIR spectra and TPD of adsorbed CO_2 indicate the presence of different types of adsorbed CO_2 species. XPS studies reveal an increase in the extent of destabilization of O 2p valence levels from Li-ETS-10 to Cs-ETS-10 systems. A strong overlap is observed between Cs 5p and O 2p valence bands. Catalytic activity of Pt supported on M-ETS-10 for *n*-hexane conversion to benzene increases with the basicity of the support and the same is correlated with the FTIR, TPD, and XPS results.

1. Introduction

There has been an increasing interest in basic catalysis by inorganic porous materials and a large number of reactions have already been reported in this area. Bifunctional catalysts such as Pt supported on acidic halided aluminas are typically used in the aromatization of *n*-paraffins into aromatics (catalytic reforming).[1,2] Besides, monofunctional catalysts such as Pt supported on the nonacidic zeolite, K-LTL[3] and MgO[4] have also been reported. The monofunctional catalysts have been found to be many times more active than bifunctional catalysts in the reforming of *n*-paraffins with C-numbers less than 9.[3] Besoukhanova et al.[5] have reported that the activity of Pt-LTL exchanged with different alkali metal ions in *n*-hexane aromatization increases with increasing basicity of the alkali metal, viz., Li < Na < K < Rb < Cs. Das et al.[6] have also made a similar observation in their study of *n*-hexane aromatization over Pt supported on different alkali metal exchanged ETS-10. Similarly, Philippou et al.[7] have also reported high benzene yields over Pt−K-ETS-10 and Pt−K-ETAS-10 in the aromatization of *n*-hexane. Apart from the electronic effect of the exchanged ion, other parameters such as the structure and pore topology of the zeolites may also influence the basicity of the zeolite. It has been reported[8,9] that an inverse relationship exists between the intermediate electronegativity (S_{int})[10] and benzene yield in the aromatization of *n*-hexane on Pt-LTL-zeolite exchanged with different alkali-metal ions. S_{int} is the geometric mean of the electronegativities of all the constituent elements in the molecule (or groups of atoms). It represents the average electronegativity of the system. S_{int} is inversely related to the charge on the O^{2-} ions, the latter being a measure of the basicity of the zeolite.

In this paper, we report FTIR studies of Pt supported on alkali-metal-exchanged molecular sieves (M-ETS-10, M = Li, Na, K, Rb, Cs, and Ba) after CO_2 adsorption at room temperature (RT). We also report UV−vis, temperature-programmed desorption (TPD) of CO_2, and X-ray photoemission spectroscopy (XPS) studies of M-ETS-10. The catalytic activities of Pt-loaded M-ETS-10 molecular sieves in *n*-hexane aromatization have been examined and correlated with their basicities.

TABLE 1: Chemical Composition of Different Ion-Exchanged M-ETS-10 (M = Li, Na, K, Rb, Cs, and Ba)

molecular sieve	chemical composition	surface area, m^2/g	S_{int}	charge on O^{2-}
Li-ETS-10	$Li_{21.2}Na_{5.4}K_{3.7}(Ti_{16.21}Si_{79.74}O_{208})$	452	3.486	−0.363
Na-ETS-10	$Na_{27.2}K_{4.0}(Ti_{16.21}Si_{79.74}O_{208})$	449	3.437	−0.374
K-ETS-10	$Na_{8.6}K_{22.4}(Ti_{16.21}Si_{79.74}O_{208})$	440	3.340	−0.394
Rb-ETS-10	$Rb_{12.1}Na_{15.2}K_{3.9}(Ti_{16.21}Si_{79.74}O_{208})$	419	3.222	−0.419
Cs-ETS-10	$Cs_{10.2}Na_{16.3}K_{5.4}(Ti_{16.21}Si_{79.74}O_{208})$	388	3.140	−0.436
Ba-ETS-10	$Ba_{11.2}Na_{7.2}K_{2.3}(Ti_{16.21}Si_{79.74}O_{208})$	390	3.660	−0.326

2. Experimental Section

2.1. Catalyst Preparation. ETS-10 molecular sieves were hydrothermally synthesized by a reported procedure.[11] The molecular sieves were converted into M-ETS-10 by exchanging thrice with the required metal chloride solution (20 mL of 1 M solution/g of ETS-10 at 80 °C with stirring for 3 h). After washing with demineralized water, the samples were filtered and dried at 383 K. M-ETS-10 samples (M = Li, Na, K, Rb, Cs, and Ba) were calcined at 773 K for 4 h. Platinum (0.6 wt %) was loaded on the ion-exchanged M-ETS-10 by stirring the powder sample with an aqueous solution of $\{[Pt(NH_3)_4](NO_3)_2\}$ (10 mL/g) at 353 K for 2 h and then evaporated to dryness on a hot water bath. The Pt-loaded samples were dried at 383 K and calcined at 723 K.[6] All the characterization studies reported below were carried out on Pt-loaded M-ETS-10 samples.

2.2. Characterization. Powder X-ray diffraction (Rigaku Model D-MAX III VC) data of the zeolites revealed the samples to be highly crystalline. Elemental analyses were done by atomic absorption spectroscopy (AAS). The compositions of the ion-exchanged zeolites are reported in Table 1. UV spectra were recorded on Shimadzu UV-2550 spectrophotometer. The UV spectra were recorded in the range of 200 to 1000 nm, in the diffuse reflectance (DR) mode using $BaSO_4$ as the reference. All FTIR spectra were recorded on a Nicolet 60 SXB spec-

* To whom correspondence should be addressed. Email: siva@cata.ncl.res.in; gopi@cata.ncl.res.in.

† Present address: GE India Technology Center, Whitefield Road, Bangalore 560 066, India.

10.1021/jp0278622 CCC: $25.00
Published on Web 07/16/2003

trometer with 2 cm^{-1} resolution, averaging over 500 scans. FTIR spectra were recorded in the framework region (400−1300 cm^{-1}) in the DR mode using KBr pellets. One milligram of zeolite and 300 mg of KBr (dried) were mixed and pelletized (under 5-ton pressure) for framework DR-IR analysis. For spectra of adsorbed CO_2, self-supported wafers were used. The sample was pressed into a thin wafer (5−6 mg/cm^2), evacuated (10^{-5} Torr) at 673 K, and cooled to 298 K to record its spectrum. Ultrapure CO_2 (99.999, Linde Air) was adsorbed on the sample at 0.4 and 5 mm equilibrium pressure for 1 h, and then the spectra were recorded.

Characterization of the basicity of the M-ETS-10 zeolites was carried out by TPD (AutoChem 2910; Micromeritics) of adsorbed CO_2. Prior to the TPD studies, the catalyst sample (400 mg, oven-dried at 383 K for 16 h) was flushed with high-purity He (50 mL/min) at 773 K for 2 h. After that, the sample was cooled to RT in He and saturated by flowing highly pure CO_2 (11.1% CO_2 in He) at 303 K for 2 h. The catalyst sample was subsequently flushed with He at 313 K for 2 h to remove the physisorbed CO_2. TPD analysis was carried out from ambient temperature to 823 K at a heating rate of 10 K/min. The CO_2 concentration in the effluent stream was monitored by using a thermal conductivity detector (TCD), and the area under the peaks were integrated by the use of GRAMS-32 software, supplied with the instrument, to determine the amount of CO_2 desorbed during TPD. TCD calibration was performed by passing known volumes of CO_2. Other characterization details including surface area measurement have been reported elsewhere.[6]

Photoemission spectra were recorded on a VG Microtech Multilab ESCA 3000 spectrometer. All measurements were made at RT using a nonmonochromatized Mg Kα X-ray source ($h\nu$ = 1253.6 eV) on powder samples. Base pressure in the analysis chamber was maintained at 3−6 × 10^{-10} Torr range. The energy resolution of the spectrometer was measured from the full width at half-maximum of metallic gold, and the value obtained is better than 0.8 eV with Mg Kα radiation at a pass energy of 20 eV. Binding energy (BE) calibration was performed with Au $4f_{7/2}$ core level (83.9 eV). BE of adventitious carbon (284.9 eV) was utilized for charge correction of all core-level spectra.

2.3. Catalytic Reaction Procedure. The catalytic reactions were carried out in a fixed bed down flow tubular silica reactor (15 mm i.d.) of 35-cm length provided with a thermowell. The catalyst (2 g) was used in the form of granules (10−20 mesh) prepared by pelletizing the powder and crushing into the desired size. The catalyst was loaded such that the tip of the thermocouple (kept inside the thermowell) was at the center of the catalyst bed. The catalyst was sandwiched by inert ceramic beads, which provided a more uniform flow distribution. The top portion of the ceramic beads additionally served as a preheater zone to vaporize the feed. A condenser was attached to the outlet of the reactor, which was cooled by water circulation from a cryostat maintained at approximately 277 K.

The reactor was placed inside a temperature-controlled furnace (Geomecanique, France). The catalyst was activated in N_2 (30 mL/min) for 5h (773 K), cooled to RT, and reduced in H_2 (30 mL/min) for 5 h at 773 K prior to carrying out the reaction at the desired temperature. The feed consisted of a mixture of H_2 and *n*-hexane (molar ratio of 6:1). *n*-Hexane was fed by a syringe pump (Braun, Germany). The space velocity (WHSV based on *n*-hexane) was 2 h^{-1}. The reaction products were analyzed in a Hewlett-Packard (model 5880) chromatograph, equipped with a 50 m capillary column (HP-5) and a flame ionization detector. Product identification was carried out by comparing with standards.

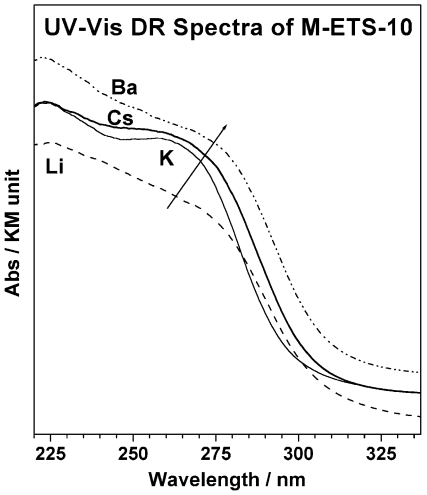

Figure 1. UV−vis diffuse reflectance spectra of M-ETS-10 molecular sieve zeolites. Solid arrow indicates the red shift in absorption maximum.

3. Results and Discussion

The chemical composition and surface area are presented in Table 1. The intensities of the X-ray diffraction lines of the as synthesized samples were slightly larger than those from the calcined samples. The intensities for the cation-exchanged samples decreased slightly in the order Li > Na ≅ Mg > K ≅ Rb > Ba > Cs-ETS-10, as reported by earlier workers.[12] The basicity of the different M-ETS-10 samples is directly related to the charge on the oxygen and inversely related to their average intermediate electronegativity (S_{int}).[10,13] The values of charge on oxygen and S_{int} for the different samples are also presented in Table 1.

3.1. Ultraviolet Spectroscopy. The DR spectra in the UV−visible region of M-ETS-10 are presented in Figure 1. The broad absorption between 250 and 300 nm suggests the presence of Ti^{4+} in octahedral (O_h) coordination.[14] M-ETS-10 samples exhibit a red shift of the absorption band from 260 nm for Li to 275 nm for Cs and 279 nm for Ba cations. These bands are associated with the $O^{2-} \rightarrow Ti^{4+}$ charge-transfer transition.[14] In contrast, this charge-transfer band is centered at ∼200 nm in TS-1,[15] where Ti is in tetrahedral (T_d) coordination and in O_h coordination at ∼255 nm in ETS-4,[16] a small pore analogue of ETS-10.

3.2. FTIR Spectroscopy of ETS-10 in the Framework Region. FTIR spectra of M-ETS-10 in the framework vibration range (400−1300 cm^{-1}) are shown in Figure 2. The M-ETS-10 samples show bands at 1058, 1060, 1062, 1063, 1065, and 1070 cm^{-1} for Li, Na, K, Rb, Cs, and Ba, respectively. Figure 2 shows the characteristic ETS-10 vibrations at 785, 745, 708, 508, and 447 cm^{-1} and shoulders at ∼1190 and ∼985 cm^{-1} as reported earlier.[17−20] The FTIR spectra of ETS-10 reported by Yang et al.[20] are similar to those reported here. The prominent bands shift toward higher frequencies on cation exchange from Li to Cs (Figure 2). The cation present in the vicinity of the anionic oxygen of the framework in the *n*-membered ring interacts electrostatically and leads to a concomitant reduction in the Si−O and Ti−O bond strength in the ring. The greater the charge transfer from O^{2-} to the cations, the weaker the (T−O) bond, and hence the observed shift in the vibrational band positions.

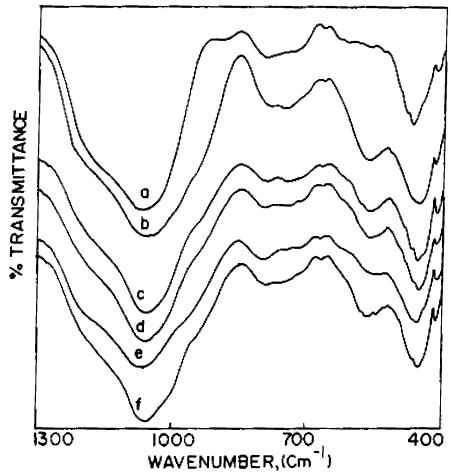

Figure 2. FTIR spectra of the framework region (a) Li-, (b) Na-, (c) K-, (d) Rb-, (e) Cs-, and (f) Ba-ETS-10.

3.3. IR Spectroscopy of Adsorbed CO_2. CO_2, being amphoteric, can be used to monitor both Lewis acid and Lewis base centers on metal oxides and zeolite surfaces. The IR spectrum of adsorbed CO_2 varies distinctly from the gas-phase spectrum and three types of bands have been observed depending on the extent of interaction of CO_2 and catalysts.[21−23] Asymmetric stretching of adsorbed CO_2 (ν_3) and carbonate vibrations are observed at about 2350 cm^{-1} and between 1800 and 1200 cm^{-1}, respectively.[20] FTIR spectra of adsorbed CO_2 on M-ETS-10 molecular sieves are shown in Figure 3, wherein the ν_3 vibration of physisorbed CO_2 is seen. ν_3 decreases from 2356 cm^{-1} for Li-MTS-10 to 2342 cm^{-1} for Cs-ETS-10 and 2346 cm^{-1} for Ba-ETS-10. The interaction of chemisorbed CO_2 is believed to be through transfer of electronic charge to the CO_2 molecule from the oxygen of ETS-10 and the above interaction increases with the size of the alkali ion. As the ionic radii of the alkali-metal cations and the metal−oxygen bond length increase, the electron donating ability of oxygen (to adsorbed CO_2) increases and hence the ν_3 shifts to lower wavenumbers. This is clearly shown in Figure 4, where the ionic radius is plotted against ν_3. This also indicates that the basicity increases with increasing cation size in the following order: Li < Na < K < Rb < Cs. Besides, the simultaneous interaction of the alkali cation and O^{2-} anion with adsorbed CO_2 may also be taking place.

The FTIR spectra of CO_2 adsorbed on M-ETS-10 in the carbonate vibrations region (chemisorbed CO_2, 1800−1275 cm^{-1}) indicates two sets of bands (spectra not shown), each set consisting of bands due to antisymmetric and symmetric stretching.[24] The frequencies of these bands for M-ETS-10 are presented in Table 2. Interestingly, unlike the ν_3 band, the change in band position is marginal from Li to Cs. Bonelli et al.[25] have concluded from FTIR, adsorption microcalorimetry, and quantum chemical calculations that cation−CO_2 interaction alone cannot account for the nature of the spectra of adsorbed CO_2 on such samples, and the presence of nearby framework anionic O^{2-} should also be considered. Their calculations showed that in the series from Li^+ to Cs^+, the cation becomes a progressively weaker Lewis acid for CO_2 adsorption; simultaneously the adjacent anionic framework becomes a progressively stronger base causing internal compensation. This type of internal compensation is probably responsible for the small change in the frequency of the major type I CO_3 band (Table 2). The large $\Delta\nu$ suggesting a bidentate type of adsorption further corroborates this view. Solymosi and Knözinger[23] have proposed $\Delta\nu$ values of 0, 100, 300, and >400 cm^{-1} for symmetrical, monodentate, bidentate, and bridged confirmations of adsorbed CO_2 species, respectively, on interacting surfaces.

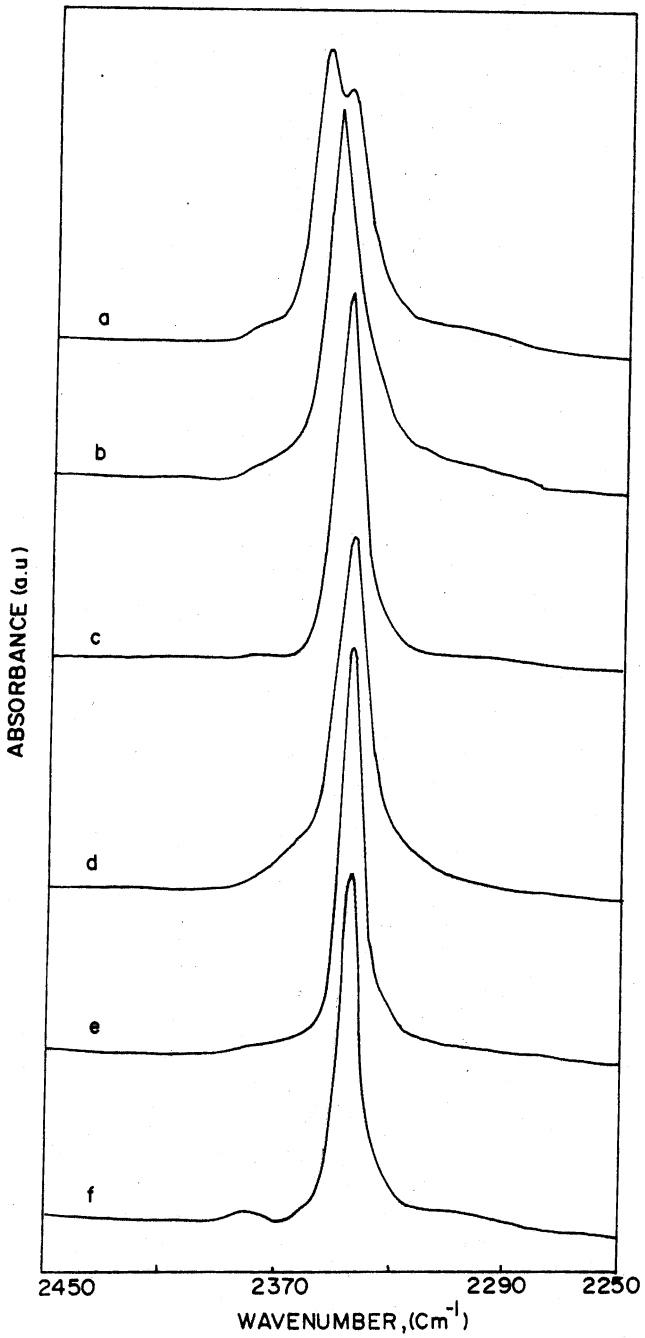

Figure 3. FTIR spectra of physisorbed CO_2 at room temperature on M-ETS-10 [M = (a) Li, (b) Na, (c) K, (d) Rb, (e) Cs, and (f) Ba] at 5-mm equilibrium pressure of CO_2.

The relative band intensity of adsorbed CO_2 between 1800 and 1200 cm^{-1} in the FTIR spectra at 0.4 and 5 mm equilibrium pressure observed over different cation exchanged samples are presented in Table 3. The intensities decreases marginally with decrease in CO_2 equilibrium pressure, but the bands persist even after evacuation up to 10^{-5} Torr. Going by the relative intensities of the IR bands, basicity increases with increasing electropositive nature of the exchanged cation, Li to Cs. However, in view of the difficulty in quantitatively exchanging all parent Na and K ions present in ETS-10 by other ions, it is difficult to quantify basicity based on the concentration of the exchanged ions in the samples. Besides, contribution from other factors (to the IR

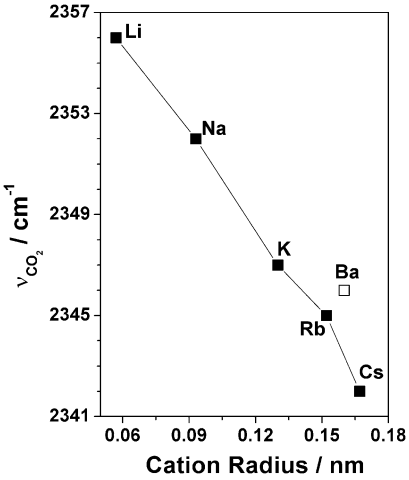

Figure 4. Correlation between ν_3 stretching frequency of adsorbed CO_2 (at 0.4-mm equilibrium pressure) and the radius of the ion-exchanged cation in the M-ETS-10 system.

TABLE 2: Frequencies of Bands for Different Forms of Carbonate Species Formed on M-ETS-10 Molecular Sieves

	type I (antisymmetric)			type II (symmetric)		
samples	cm^{-1}	cm^{-1}	$\Delta\nu$	cm^{-1}	cm^{-1}	$\Delta\nu$
Li-ETS-10	1651	1339	312	1625		
Na-ETS-10	1651	1335	316	1629		
K-ETS-10	1651	1333	318	1632		
Rb-ETS-10	1652	1330	322	1634	1279	355
Cs-ETS-10	1652	1327	325	1642	1280	362
Ba-ETS-10	1649			1625		

TABLE 3: Relative Basicity of Alkali Metal Exchanged M-ETS-10 Molecular Sieves from FTIR Studies

	rel IR intensity of chemisorbed CO_2 species at CO_2 pressure[a]			rel IR intensity of chemisorbed CO_2 species at CO_2 pressure[a]	
samples	0.4 mm	5 mm	samples	0.4 mm	5 mm
Li-ETS-10	78	84	Rb-ETS-10	120	129
Na-ETS-10	82	96	Cs-ETS-10	125	132
K-ETS-10	108	123	Ba-ETS-10	112	126

[a] Sum of the intensities of the bands in the range 1800−1200 cm^{-1}.

intensity) also like changes in mode of CO_2 adsorption and molar absorption coefficient of the different adsorbed species should also be taken into account. In any case, the distinct increase in the observed IR intensities does reveal an increase in basicity of the samples on going from Li to Cs.

3.4. Temperature-Programmed Desorption of Adsorbed CO_2. CO_2 is frequently used as a probe molecule in TPD to determine basicity due to its small molecular size, stability, and weak acidic character.[26,27] Representative TPD plots of CO_2 desorption from M-ETS-10 samples are shown in Figure 5. It is apparent from the broadening of the TPD peak on the high-temperature side that at least two types of adsorbed species are present. TPD plots were deconvoluted to separate the two types of adsorbed CO_2 species and the details are given in Table 4. It is found that the amount of CO_2 adsorbed increases from Li to Cs, in agreement with the IR results on increase in basicity. The CO_2 uptake (on a constant weight basis) increases for the cation-exchanged samples in the order: Li < Na ≅ K < Rb < Cs and Ba. In addition, the temperatures of the peak maximum of the deconvoluted peaks are considerably larger in the cases of Cs and Ba, compared to the other elements.

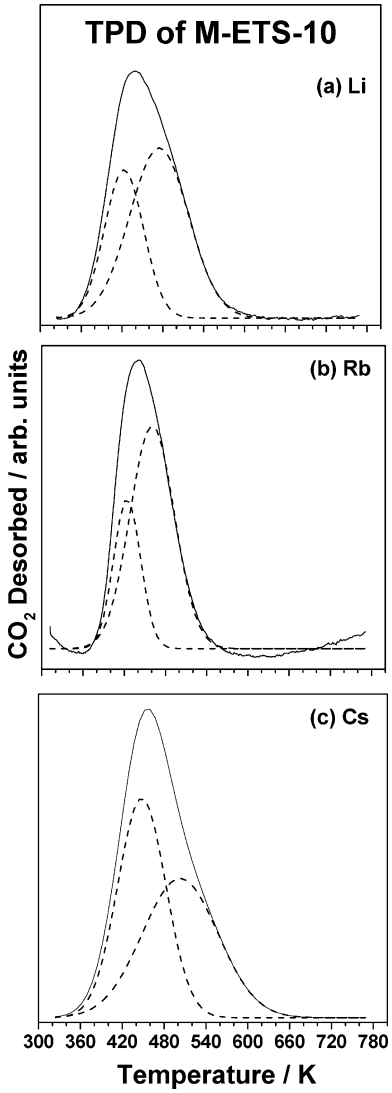

Figure 5. Representative TPD profiles of CO_2 desorption from M-ETS-10. The deconvoluted curves are shown as dotted lines: (a) Li, (b) Rb, and (c) Cs.

TABLE 4: TPD Data Obtained over Different Alkali and Alkaline-Earth Metal Exchanged ETS-10

	temp of peak max, K		CO_2 adsorbed
M	major peak	minor peak	(desorbed), mmol/g
Li-ETS-10	474	422	57.4
Na-ETS-10	476	425	62.3
K-ETS-10	476	425	66.5
Rb-ETS-10	463	422	105.5
Cs-ETS-10	503	449	132.1
Ba-ETS-10	555	470	107.3

3.5. Photoelectron Spectroscopy Analysis. XPS were recorded on M-ETS-10 samples for valence band (VB), Si 2p, Ti 2p, and O 1s core levels. Figure 6 displays (a) VB and (b) O 1s core level spectra of the M-ETS-10 system. The VB spectrum of MCM-41 (SiO_2) is given for comparison. The following interesting observations are made: (1) The BE of O 2p bands decreases from Li to Cs/Ba through Na and Rb cases. (2) The energy gap between O 2p and O 1s bands increases by 1 eV from 525 to 526 eV for Li and Cs/Ba, respectively, through Na and Rb cases. (3) The Cs 5p band observed at 11.3 eV overlaps with the two topmost O 2p derived bands in the energy range between 8 and 14 eV in Cs-ETS-10. (4) Rb 4p and Ba 5p levels appear at 14.3 and 15 eV, respectively, indicates that there is large overlap between the above bands and the O 2p derived

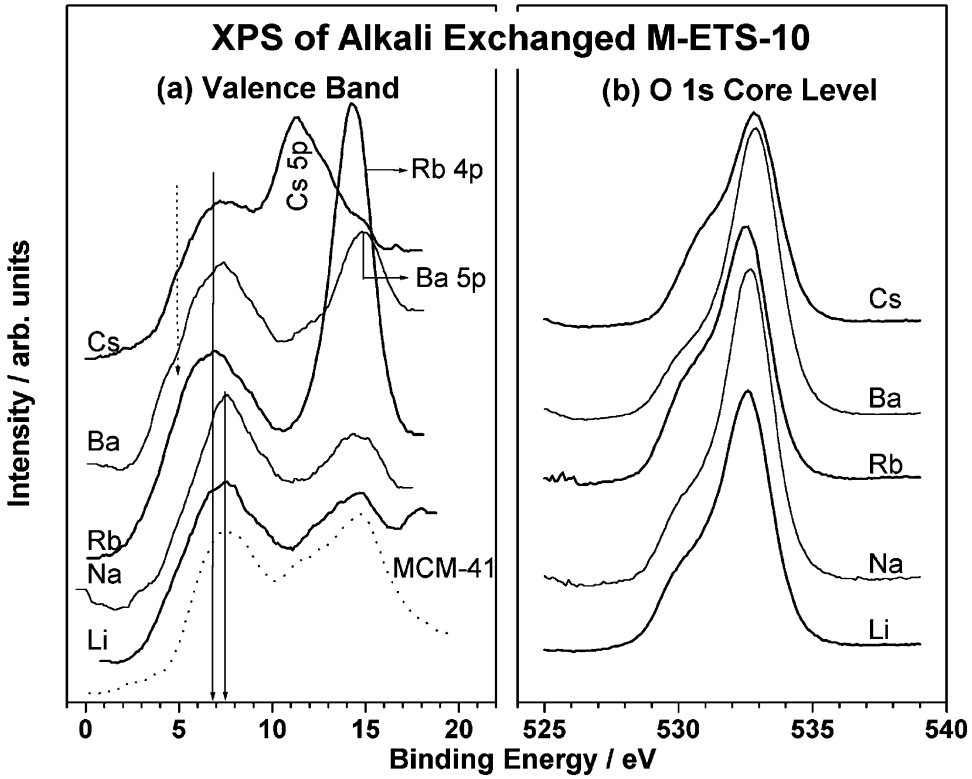

Figure 6. X-ray photoelectron spectra of M-ETS-10 catalysts for (a) valence band and (b) O 1s core level regions. VB spectrum from MCM-41 is also displayed for comparison. BE of the topmost O 2p band decreases from Li to Cs. Note the overlap in Cs 5p band with O 2p bands and low BE shoulder appearance in the topmost band in the Ba- and Cs-ETS-10 cases.

band around 15 eV. (5) There is also a low BE shoulder appearing around 5 eV in the topmost O 2p band (dotted arrow in Figure 6a), only in the Cs and Ba cases. The BE of O 1s orbital increases from Li to Cs marginally. Two types of O 1s peaks can be expected due to the oxygen linkages in Si−O−Si and Si−O−Ti and another due to the Ti−O−Ti linkage. The high-intensity peak at a high BE around 532−533 eV is attributed to O in Si−O−Si and Si−O−Ti linkages, and the low BE feature with low intensity is due to that of Ti−O−Ti (the Si/Ti ratio of the samples is ∼5). Si 2p and Ti 2p core levels do not show a significant change with different cations.

A comparison of the MCM-41 spectrum, which is essentially silica, and Li/Na/K-ETS-10 spectrum clearly indicates that the main VB features are exclusively derived from the O 2p features. VB results for Li, Na, and K cases show two O 2p derived bands at about 7 and 14.5 eV, and there is no energy overlap between the above alkali ion bands and the O 2p bands. However, Rb and Ba display 4p and 5p shallow core levels, respectively, which overlap with that of the O 2p band at 14.5 eV. The high intensity of the Rb 4p−O 2p feature is partly due to the higher photoionization cross section of Rb 4p[28] and partly due to close BE overlap of both Rb 4p and O 2p bands. On the other hand, the BE of the Cs 5p band (11.3 eV) is such that it interacts well with both the topmost O 2p bands, indicating the effective interaction with the support. Further, the shoulder appearing at 5 eV in Cs and Ba cases suggests an effective electronic interaction of Cs/Ba with ETS-10. Although no separate shoulder is visible in the Rb case, the broadening of the topmost O 2p band hints at a similar interaction. The shoulder at 5 eV is attributed to the overlap of an alkali-metal ion valence band with that of O 2p bands. It is known that the nature of the topmost energy band in the VB dictates the physicochemical properties and activities of the catalysts,[29] and in this respect the better catalytic activity associated with the Cs- and Ba-ETS-10 system (vide infra) is in good agreement with XPS results.

XPS results are also in good agreement with TPD, IR, S_{int}, and oxygen charge calculation results (Table 1) on the increase in basicity from Li to Cs/Ba. The high BE of O 2p bands and the small energy gap between O 2p and O 1s in Li/Na clearly demonstrate the presence of stabilized oxygen-derived VBs compared to destabilized VBs in the Cs and Ba cases. Appearance of a shoulder at 5 eV and its destabilized nature clearly demonstrate an increase in the charge-donating ability of Cs and Ba and hence higher basicity. A comparatively large basicity is observed for Cs- and Ba-ETS-10 systems in TPD as well as IR in terms of large amount of CO_2 chemisorbed (and large intensity of the IR bands).

3.6. Catalytic Activity. *n*-Hexane aromatization was carried out over various Pt-loaded alkali-metal-exchanged zeolite samples in order to evaluate the influence of the alkali-metal ion on the catalytic activity. The *n*-hexane aromatization activities of a series of Pt-M-ETS-10 catalysts are presented in Table 5. It is noticed that the more basic catalysts are more active in *n*-hexane conversion and benzene selectivity as reported earlier.[6,7,30] The activity increases linearly with increase in the electropositive nature of the exchanged metal cation in the order Li < Na < K < Rb < Cs and Ba. In the case of the alkaline catalysts, benzene yield increases with the basicity from 1.3% for Pt−Li-ETS-10 to 39.5% for Pt−Cs-ETS-10. The C_1−C_5 yield also increases with the basicity of the sample, being 2.5% in the case of Li and 16.2% in the case of Cs. The hydrogenolysis activity (C_1−C_5 formation) of Pt is more when supported on basic ETS-10; this is especially apparent over the alkali-exchanged catalysts. It is also interesting to note that the more basic catalyst (Pt−Cs-ETS-10) possess slightly larger isomerization activity than the less basic ones (Pt−Li-ETS-10). The increased isomerization activity with basicity suggests that

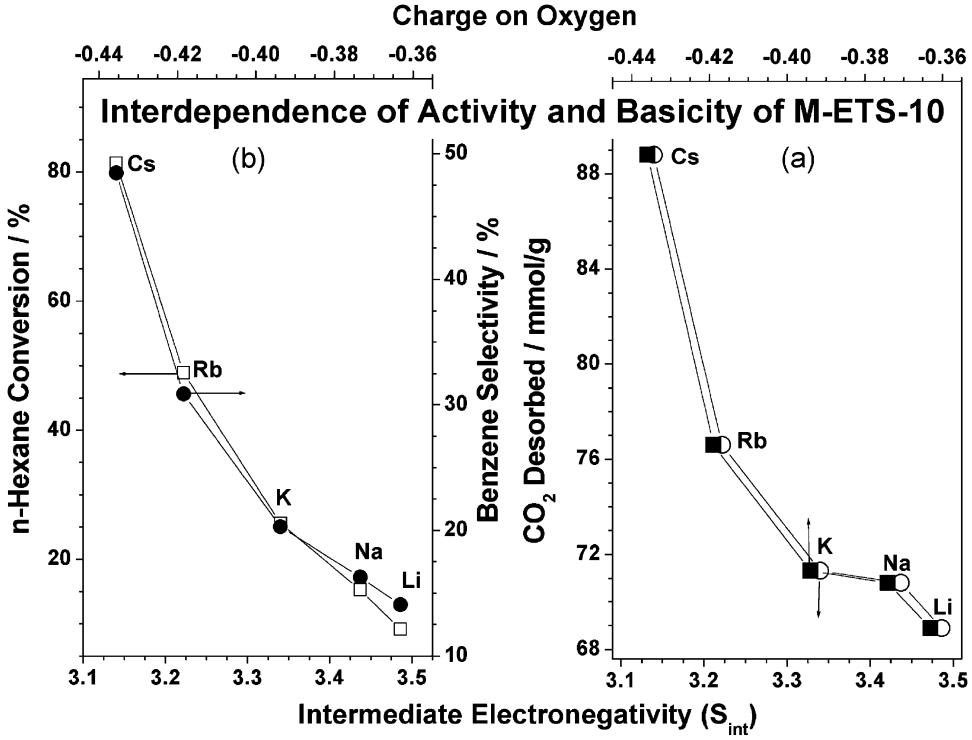

Figure 7. (a) Relationship between CO_2 desorbed (in TPD) and S_{int} and the charge on the oxygen atoms in M-ETS-10. (b) Interdependence of the catalytic activity of alkali-ion-exchanged M-ETS-10, S_{int}, and the charge on oxygen. A high degree of linearity demonstrates a hand-in-hand change of the above parameters in a and b.

TABLE 5: Comparison of *n*-hexane Aromatization Activity of ETS-10 Molecular Sieve[a]

	M in Pt-M-ETS-10 (Pt = 0.6%)					
product yield, wt %	Li	Na	K	Rb	Cs	Ba
conversion (%)	9.2	15.3	25.6	48.9	81.4	85.9
C_1 to C_5	2.5	3.9	6.9	11.7	16.2	4.8
i-C_6[b]	0.7	0.9	1.2	1.3	2.3	3.4
methylcyclopentane	0.4	0.5	0.7	1.7	4.3	10.9
benzene	1.3	2.5	5.2	15.1	39.5	52.1
benzene selectivity (%)[c]	14.1	16.3	20.3	30.9	48.5	60.7
toluene + xylenes	0	2.3	3.1	2.2	2.0	4.5
others	4.3	5.2	8.5	16.9	17.1	10.2

[a] Reaction conditions: temp, 733 K; WHSV = 2 h^{-1}; pressure = 1 atm.; TOS = 2 h; H_2:*n*-hexane (mol) = 6:1. [b] Isohexanes, mainly 2-methylpentane and 3-methylpentane. [c] Benzene selectivity = wt of benzene/wt of all products × 100.

isomerization can occur by a monofunctional route via C_1-C_5 cyclization and ring-opening reactions over the Pt metal. The increased yield of methylcyclopentane over the more basic catalysts confirms this mechanism for isomerization. The results reveal that Pt supported on basic samples is more selective for the aromatization reaction. However, an increase in isomerization and hydrogenolysis reactions also occurs with increase in the basicity of the support.

3.7. Relationship between S_{int}, Charge on Oxygen, and Catalytic Activity. The reported calculation procedure was adopted for S_{int}[10,13] calculation and the results are presented in Table 1. Over basic supports, Pt is believed to be electron rich, arising from electron transfer from the basic O^{2-} ions in the lattice.[5,31,32] Figure 7a shows the relationship between the S_{int}, charge on oxygen atom, and the amount of CO_2 desorbed in TPD. A similar relationship between catalytic activity (both *n*-hexane conversion and benzene selectivity), oxygen charge, and S_{int} on Pt-M-ETS-10 samples is presented in Figure 7b. The relationship shown in panels a and b of Figure 7 clearly demonstrates that the catalytic activity of the Pt-M-ETS-10 molecular sieve is through the activation of Pt by the basicity of the exchanged metal. Many workers have suggested that the increased activity of Pt supported on alkali-ion-exchanged zeolites is a result of electron transfer from the basic support (O^{2-} ions) to the Pt. Ab initio calculations on the charge on Pt supported on different alkali-metal-exchanged ETS-10 have also revealed that the electronic charge on Pt increases with the basicity of the support.[24,30] A direct relationship between charge on Pt and the activity and selectivity of the catalysts in *n*-hexane aromatization was also revealed. Characterization of catalysts by XPS, IR, and TPD further confirms that indeed there is a progressive change in basicity from Li to Cs in the M-ETS-10 series. Besides, the large activity and selectivity of Cs-ETS-10 is presumably due to greater electron transfer to the Pt from the support (O^{2-} ions), this transfer being facilitated by the presence of a new low energy VB feature around 5 eV.

4. Conclusions

The physicochemical interaction between alkali-metal ions and ETS-10 support and hence the basicity are clearly brought out by many methods such as FTIR spectroscopy, TPD of adsorbed CO_2, XPS studies, and calculations of S_{int} and charge on oxygen anions. XPS investigations demonstrate the presence of destabilized O 2p valence bands in the Cs/Ba-ETS-10 system and the effective energy overlap of O 2p and alkali-metal ion bands. The above results are corroborated with the catalytic activity of the Pt-M-ETS-10 system for *n*-hexane conversion to benzene, which increases with the basicity.

Acknowledgment. We thank B.B.Tope for FTIR characterization of the samples. S.B.W. thanks CSIR, New Delhi for a research fellowship.

References and Notes

(1) *Catalytic Naphtha Reforming, Science and Technology*; Antos, G. J., Aitani, A. M., Parera, J. M., Eds. Marcel Dekker Inc.: New York, 1995.

(2) Sinfelt, J. H. In *Catalysis Science and Technology*; Anderson, J. R., Boudart, M., Eds.; Springer-Verlag: Berlin, 1981; Vol. 1, p 257.
(3) Bernard, J. R. *Proc. 5th Int. Conf. Zeolites*; Rees, L. V. C., Ed.; Heyden: London, 1980; p 686.
(4) Davis, R. J.; Derouane, E. G. *Nature* **1991**, *349*, 313.
(5) Besoukhanova, C.; Guidot, J.; Barthomeuf, D.; Breysse, M.; Bernard, J. R. *J. Chem. Soc. Faraday Trans. 1* **1981**, *77*, 1595.
(6) Das, T. K., Chandwadkar, A. J.; Sivasanker, S. *Stud Surf Sci. Catal.* **1998**, *113*, 455.
(7) Philippou, A.; Naderi, M.; Pervaiz, N.; Rocha, J.; Anderson, M. W. *J. Catal.* **1998**, *178*, 174.
(8) Barthomeuf, D. *Stud. Surf. Sci. Catal.* **1991**, *65*, 157.
(9) Larsen, G.; Haller, G. L. *Catal. Lett.* **1989**, *3*, 1003.
(10) Mortier, W. J. *J. Catal.* **1978**, *55*, 138.
(11) Das, T. K.; Chandwadkar, A. J.; Sivasanker, S. *J. Chem. Soc., Chem. Commun.* **1996**, 1105.
(12) Engelhardt, J.; Szanyi, J.; Valyon, J. *J. Catal.* **1987**, *107*, 296.
(13) Sanderson, R. T. *Chemical Bonds and Bond Energy*; Academic Press: New York, 1976.
(14) Jacobs P. A. *DGMK Tagenbericht* **1992**, *171*, 9204.
(15) Astorino, E.; Peri, J. B.; Willey, R.; Busca, G. *J. Catal.* **1995**, *157*, 482.
(16) Armaroli, T.; Busca, G.; Milella, F.; Bregani, F.; Toledo, G. P.; Nastro, A.; De Luca, P.; Bagnasco, G.; Turco, M. *J. Mater. Chem.* **2000**, *10*, 1699.
(17) Das, T. K.; Chandwadkar, A. J.; Budhkar, A. P.; Belhekar, A. A.; Sivasankar, S. *Micropor. Mater.* **1995**, *4*, 195.
(18) Valchev, V.; Mintova, S. *Zeolites* **1994**, *14*, 697.
(19) Valtchev, V. *Chem. Commun.* **1994**, 261.
(20) Yang, X.; Paillaud, J.-L.; van Breukelen, H. F. W. J.; Kessler, H.; Dupery, E. *Micropor. Mesopor. Mater.* **2001**, *46*, 1.
(21) Nakamoto, K. In *Infrared and Raman Spectra of Inorganic and Coordination Compounds*, 3rd ed.; Wiley: New York, 1978; p 243.
(22) Bussca, G.; Lorenzeli, V. *Mater. Chem.* **1982**, *7*, 89.
(23) Solymosi, F.; Knözinger, H. *J. Catal.* **1990**, *122*, 166.
(24) Waghmode, S. B. Aromatization of alkanes over Pt incorporated molecular sieves: Catalytic and molecular modeling studies. Ph.D. Thesis, University of Pune, May 2002.
(25) Bonelli, B.; Civalleri, B.; Fubini, B.; Ugliengo, P.; Arean, C. O.; Garrone, E. *J. Phys. Chem. B* **2000**, *104*, 10978.
(26) Parkyns, N. D. *J. Phys. Chem.* **1971**, *75*, 526.
(27) Morterra, B.; Zecchina, A.; Coluccia, S. *Faraday Trans.* **1977**, 1544.
(28) Yeh, J. J.; Lindau, I. *At. Data Nucl. Data Tables* **1985**, *32*, 1.
(29) Velu, S.; Suzuki, K.; Gopinath, C. S. *J. Phys. Chem. B* **2002**, *106*, 12737.
(30) Waghmode, S. B.; Das, T. K.; Vetrivel, R.; Sivasanker, S. *J. Catal.* **1999**, *185*, 265.
(31) Han, W. J.; Kooh, A. B.; Hicks, R. F. *Catal. Lett.* **1993**, *18*, 193.
(32) Barthomeuf, D.; de Mallmann, A. *Stud. Surf. Sci. Catal.* **1988**, *37*, 365.